Video Article

Simultaneous Measurement of Superoxide/Hydrogen Peroxide and NADH Production by Flavin-containing Mitochondrial Dehydrogenases

Ryan J. Mailloux[1], Adrian Young[1], Marisa O'Brien[1], Robert Morris Gill[1]

[1]Department of Biochemistry, Memorial University of Newfoundland

Correspondence to: Ryan J. Mailloux at rjmailloux@mun.ca

URL: https://www.jove.com/video/56975
DOI: doi:10.3791/56975

Keywords: Biochemistry, Issue 132, Reactive oxygen species, hydrogen peroxide, NADH, flavin-dependent dehydrogenases, alpha-ketoglutarate dehydrogenase complex, pyruvate dehydrogenase complex, microplate fluorometry, enzyme activity, mitochondria

Date Published: 2/24/2018

Citation: Mailloux, R.J., Young, A., O'Brien, M., Gill, R.M. Simultaneous Measurement of Superoxide/Hydrogen Peroxide and NADH Production by Flavin-containing Mitochondrial Dehydrogenases. *J. Vis. Exp.* (132), e56975, doi:10.3791/56975 (2018).

Abstract

It has been reported that mitochondria can contain up to 12 enzymatic sources of reactive oxygen species (ROS). A majority of these sites include flavin-dependent respiratory complexes and dehydrogenases that produce a mixture of superoxide ($O_2^{\bullet-}$) and hydrogen peroxide (H_2O_2). Accurate quantification of the ROS-producing potential of individual sites in isolated mitochondria can be challenging due to the presence of antioxidant defense systems and side reactions that also form $O_2^{\bullet-}$/H_2O_2. Use of nonspecific inhibitors that can disrupt mitochondrial bioenergetics can also compromise measurements by altering ROS release from other sites of production. Here, we present an easy method for the simultaneous measurement of H_2O_2 release and nicotinamide adenine dinucleotide (NADH) production by purified flavin-linked dehydrogenases. For our purposes here, we have used purified pyruvate dehydrogenase complex (PDHC) and α-ketoglutarate dehydrogenase complex (KGDHC) of porcine heart origin as examples. This method allows for an accurate measure of native H_2O_2 release rates by individual sites of production by eliminating other potential sources of ROS and antioxidant systems. In addition, this method allows for a direct comparison of the relationship between H_2O_2 release and enzyme activity and the screening of the effectiveness and selectivity of inhibitors for ROS production. Overall, this approach can allow for the in-depth assessment of native rates of ROS release for individual enzymes prior to conducting more sophisticated experiments with isolated mitochondria or permeabilized muscle fiber.

Video Link

The video component of this article can be found at https://www.jove.com/video/56975/

Introduction

The ultimate goal of nutrient metabolism is to make adenosine triphosphate (ATP). In mammalian cells, this occurs in mitochondria, double-membraned organelles that convert the energy stored in carbon into ATP. The production of ATP begins when carbon is combusted by mitochondria forming two electron carriers, NADH and flavin adenine dinucleotide ($FADH_2$)[1]. NADH and $FADH_2$ are then oxidized by multi-subunit respiratory complexes I and II, respectively, and the liberated electrons are ferried to the terminal electron acceptor molecular oxygen (O_2) at complex IV[1]. The thermodynamically favorable "downhill" transfer of electrons to O_2 at the end of the chain is coupled to the export of protons into the intermembrane space by complexes I, III, and IV. This creates a transmembrane electrochemical gradient of protons (proton-motive force), a temporary form of Gibbs free energy that is tapped by complex V to make ATP[2]. Electron transfer reactions in mitochondria are not perfectly coupled to ATP production. At various points in the Krebs cycle and the respiratory chain, electrons can prematurely interact with O_2 to form ROS[3]. The most biologically relevant ROS generated by mitochondria are $O_2^{\bullet-}$ and H_2O_2. Although $O_2^{\bullet-}$ is often considered the proximal ROS formed by mitochondria, it is now evident that sites of production form a mixture of $O_2^{\bullet-}$ and H_2O_2, which is associated with the free radical chemistry of flavin prosthetic groups[4,5]. At high levels, ROS can be dangerous, damaging biological constituents required for cell function resulting in oxidative distress[6]. However, at low amounts, mitochondrial ROS fulfill vital signaling functions. For instance, H_2O_2 release from mitochondria has been implicated in controlling T-cell activation, stress signaling (*e.g.*, induction of Nrf2 signaling pathways), the induction of cell proliferation and differentiation, insulin signaling and release, and feeding behavior[7]. Considerable progress has been made in understanding the signaling function of ROS. However, important questions still remain in regard to which enzymes in mitochondria serve as the most important sources and how production is controlled.

ROS release by a site of production depends on several factors: 1) the concentration of the electron donating site, 2) the redox state of the electron donating site, 3) access to oxygen, and 4) the concentration and type of oxidation substrate[3,8,9]. In mitochondria, other factors like the concentration of NADH and membrane potential strength also influence ROS production[8,10]. For example, the rate of $O_2^{\bullet-}$/H_2O_2 production by purified PDHC or KGDHC increases with increasing NADH availability[5,11]. In this scenario, electrons are flowing backwards from NADH to the FAD center in the E_3 subunit of PDHC or KGDHC, the site for $O_2^{\bullet-}$/H_2O_2 production[12]. Similarly, the provision of NAD^+ has the opposite effect, decreasing ROS release from KGDHC[12]. Thus, controlling entry or exit of electrons from sites of ROS production can alter how much $O_2^{\bullet-}$/H_2O_2 is formed. For instance, blocking the E_2 subunit of PDHC or KGDHC with CPI-613, a lipoic acid analog, results in an almost 90% decrease in $O_2^{\bullet-}$/H_2O_2 production[13]. Similar results can be obtained with the chemical S-glutathionylation catalysts, diamide and disulfiram, which almost abolish $O_2^{\bullet-}$/H_2O_2 production by PDHC or KGDHC via the conjugation of glutathione to the E_2 subunit[14]. The trade-off for blocking electron flow

through the E_2 subunit of PDHC and KGDHC is a decrease in NADH production which diminishes ROS formation by the electron transport chain (*e.g.*, complex III). This can also decrease ATP output by the electron transport chain. Overall, blocking electron entry to sites of ROS production can be a highly effective means of controlling $O_2^{\bullet-}/H_2O_2$ production.

Mitochondria can contain up to 12 potential $O_2^{\bullet-}/H_2O_2$ sources[6]. Most of these sites are flavin-containing enzymes which generate a mixture of $O_2^{\bullet-}$ and H_2O_2. Use of different substrate and inhibitor combinations have allowed for the identification of which respiratory complexes and mitochondrial dehydrogenases serve as high capacity $O_2^{\bullet-}/H_2O_2$ forming sites in different tissues[3]. PDHC and KGDHC have been shown to serve as high capacity $O_2^{\bullet-}/H_2O_2$ emitting sites in muscle and liver mitochondria[13,15]. However, some difficulties remain in regard to the examination of the $O_2^{\bullet-}/H_2O_2$ forming potential of individual sites in mitochondria and the impact that different substrate and inhibitor combinations have on the activities of the enzymes. This is due to the presence of unwanted side reactions (*e.g.*, formation of $O_2^{\bullet-}/H_2O_2$ by sites other than the enzyme of interest), contaminating endogenous nutrients (*e.g.*,*fatty acids) or organelles (e.g.*, peroxisomes which also form $O_2^{\bullet-}/H_2O_2$), and use of inhibitors that lack selectivity, and/or use of compounds that do not fully inhibit ROS production. Certain inhibitors can also alter the mitochondrial bioenergetics and direction of electron flow, and this alters ROS release from other sites of production and confounds results. Absolute rates for $O_2^{\bullet-}/H_2O_2$ release from individual sites in mitochondria are also difficult to quantify due to the high concentration of $O_2^{\bullet-}$ and H_2O_2 eliminating enzymes in the matrix and intermembrane space. Therefore, elimination of any competing reactions that can interfere with $O_2^{\bullet-}/H_2O_2$ release measurements can be useful when identifying high capacity $O_2^{\bullet-}/H_2O_2$ forming sites.

Here, we present a simple method that allows for the simultaneous examination of $O_2^{\bullet-}/H_2O_2$ production and NADH formation by purified flavin-dependent dehydrogenases. By using purified enzymes, unwanted ROS forming side reactions and ROS degrading enzymes can be eliminated allowing for a more accurate measure of native $O_2^{\bullet-}/H_2O_2$ production rates for individual flavoenzymes. This method can be used to directly compare the $O_2^{\bullet-}/H_2O_2$ forming capacity of different purified dehydrogenases or to screen potential site-specific inhibitors for $O_2^{\bullet-}/H_2O_2$ release. Finally, measuring $O_2^{\bullet-}/H_2O_2$ and NADH production simultaneously can allow for a real-time assessment of the relationship between enzyme activity and ROS release capacity.

Protocol

1. Chemicals and Purified Enzymes

1. Procure the following materials: PDHC and KGDHC of porcine heart origin (or another purified mitochondrial flavoenzyme); H_2O_2 (30% solution), pyruvate, α-ketoglutarate, NAD^+, NADH, CoASH, thiamine pyrophosphate (TPP), mannitol, HEPES, sucrose, EGTA, 3-methyl-2-oxo valeric acid (KMV), superoxide dismutase (SOD), horseradish peroxidase (HRP), 10-Acetyl-3,7-dihydroxyphenoxazine reagent (AUR), and CPI-613.

2. Planning the Assay and Reagent Preparation

1. Set up the assay according to **Table 1** in a 96-well plate.
   NOTE: The total volume for each reaction is 200 µL. Stock concentrations are adjusted such that 20 µL of reagent is added to each well. This ensures rapid addition of cofactors and substrates to each reaction well prior to starting the assay.
2. Prepare reaction buffer containing 220 mM mannitol, 70 mM sucrose, 1 mM EGTA, and 20 mM HEPES (pH 7.4 with HCl).
   NOTE: This could change depending on the physical properties of different purified enzymes.
3. Examine the purified KGDHC or PDHC for contamination using enzyme activity assays[14,16,17] or by immunoblot or Coomassie stain[5].
4. Prepare all reagents in the reaction buffer as per the working solution concentrations in **Table 1**.
5. Store all reagents as 1 mL aliquots at -20 °C. Store pyruvate and α-ketoglutarate at -80 °C in 100-µL aliquots to prevent spontaneous degradation due to auto-oxidation and repeated freeze-thaw.
6. Prepare the AUR reagent master stock in 1 mL of DMSO and then dilute to 100 µM in reaction buffer. Store protected from light.
   NOTE: Here, the 100 µM working solution is made fresh every 2 to 3 weeks and protected from light.

3. Setting Up the Assay Template

1. Set up the assay procedure on a monochromatic microplate reader with dual measurement capabilities.
2. Define the reading procedure by selecting "PROTOCOL". Then click "PROCEDURE".
3. Set "TEMPERATURE" to 25 °C (**Figure 1A**).
4. Click "START KINETIC" to set read conditions (**Figure 1A**). Set the time and number of read intervals/experiments.
5. Click "READ" (**Figure 1B**).
   NOTE: Samples are read from TOP position with a gain of 50. Time: 5 min, read at 30-s intervals. Channel 1: Resorufin fluorescence - excitation/emission = 565 nm:600 nm, wavelength width of 13.5 nm. Channel 2: NADH autofluorescence - excitation/emission = 376 nm:450 nm, wavelength width of 20 nm.
6. Under "READ", select wells to monitor (*e.g.*, A1-A4 and B1-B4).
7. Select "END KINETIC".

4. Standard Curves

1. Thaw the reagents and store on ice until needed.
2. **NADH standard curve (Figure 2A)**
   1. Prepare the working solutions for NADH in the concentration range of 0.5-10 mM in reaction buffer.
   2. Add 20 µL aliquots from each NADH working solution concentration to wells containing 180 µL reaction buffer. The final concentration of NADH in each well is 0.05-1 mM.

3. Click "READ" and set excitation/emission = 376 nm:450 nm, wavelength width of 20 nm.
   NOTE: This is an endpoint read only - kinetic parameters are not required.

3. **AUR standard curve (Figure 2B)**
   1. Prepare the working stocks of hydrogen peroxide in reaction buffer; stock concentrations range from 200-4,000 nM.
   2. Add 120 µL of the reaction buffer to each well.
   3. Add 20 µL of HRP (working stock concentration = 30 U/mL, final concentration in the well = 3 U/mL), 20 µL of SOD (working stock concentration = 250 U/mL, final concentration in the well = 25 U/mL), and 20 µL of AUR (working stock concentration = 100 µM, final concentration in the well = 10 µM) to each well containing reaction buffer.
   4. Add 20 µL of each H_2O_2 working stock solution to each well containing buffer and assay reagents. The final reaction volume is 200 µL and the final concentration of H_2O_2 in each well is 20-400 nM.
   5. Incubate the plates for 1 min in the plate reader at 25 °C.
   6. Click "READ" and set excitation/emission = 565 nm/600 nm, wavelength width of 13.5 nm. Note that this is an endpoint read only - kinetic parameters are not required.

5. Measuring $O_2^{\bullet-}$ /H_2O_2 Release and NADH Production by KGDHC and PDHC

1. See **Table 1** for the order of addition of the different reagents, the concentration of each working solution, and the volume added to each well.
2. Add 40 µL of reaction buffer to each well. For assays using KMV or CPI-613, add 20 µL of buffer to each well.
3. Add 20 µL of PDHC or KGDHC (working stock of 1 U/mL, final concentration per well = 0.1 U/mL) to each well.
4. Incubate PDHC and KGDHC at 25 °C for 2 min.
5. Add 20 µL of KMV (working stock = 100 mM, final concentration = 10 mM) or 20 µL of CPI-613 (working stock concentration = 1.5 mM, final concentration = 150 µM) (**Table 2**).
   NOTE: This step can be excluded if inhibitors are not being used for the assays.
6. Incubate for 1 min at 25 °C.
   NOTE: This step can be excluded if inhibitors are not being used for the assays.
7. Add 20 µL of HRP (working stock concentration = 30 units/mL, final concentration in the well = 3 units/mL) and 20 µL of SOD (working stock concentration = 250 units/mL, final concentration in the well = 25 units/mL) to each well.
8. Add 20 µL of coenzyme A (working stock concentration = 1 mM, final concentration = 0.1 mM), 20 µL of TPP (working stock concentration = 3 mM, final concentration = 0.3 mM), and 20 µL of NAD^+ (working stock concentration = 10 mM, final concentration = 1 mM) to each well.
9. Remove the AUR reagent from protective tinfoil covering and add 20 µL to each well.
10. Add 20 µL of pyruvate (working stock concentration ranging from 1-100 mM, final concentration for assays = 0.1-10 mM) to wells containing PDHC and α-ketoglutarate (working stock concentration ranging from 1-100 mM, final concentration for assays = 0.1-10 mM) to wells containing KGDHC.
11. Click "READ" to start kinetic measurement.

6. Data Analysis

1. Hold down the 'CTRL' button on the keyboard and click wells to generate one graph containing all kinetic measurements corresponding to channel 1 (**Figure 3A**).
2. Click "data" in the view icon in the upper right corner for raw values for relative fluorescence units (RFU) measured at the different time points (**Figure 3B**).
3. Export the values for analysis (**Table 3**).
4. Click the "Graph" drop down menu on top right (**Figure 3B**) to access RFU values associated with the fluorescence channel 2.
5. Repeat steps 6.1 to 6.3 for channel 2.

Representative Results

Figure 3A provides a representative trace for the RFU collected during the simultaneous measurement of H_2O_2 and NADH production by purified KGDHC. The raw RFU data for each time interval is depicted in **Figure 3B**. The raw RFU data are then exported for analysis. By extrapolating from standard curves presented in **Figure 2**, the absolute amount of NADH and H_2O_2 formed at each measurement interval over the 5-min period can be determined. An example of this calculation is provided in **Table 3**. Once the amount of NADH and H_2O_2 formed by KGDHC or PDHC at the different intervals has been determined, values are copied and inputted into a graphing/statistical software for further analysis. Using the XY graph-type analysis, the amount of NADH (µmol) and H_2O_2 (pmol) formed by KGDHC or PDHC can be plotted as a function of time (**Figure 4A**). Using these values, the rate of NADH and H_2O_2 formation during substrate oxidation can also be calculated. As shown in **Figure 4B**, KGDHC and PDHC display different characteristics in terms of NADH and H_2O_2 forming capability.

Once it has been established that KGDHC and PDHC are enzymatically active and NADH and H_2O_2 formation can be tracked simultaneously, ROS release properties and enzyme activities can be measured. We chose to compare KGDHC and PDHC since they are highly homologous in basic structure and have been documented to be high capacity sites for ROS production[5]. **Figure 5** and **Figure 6** demonstrate the dependency of NADH and H_2O_2 production on substrate concentration. PDHC is easily saturated by low amounts of substrate with the rate of NADH and H_2O_2 production reaching its maximum at 0.1-0.5 mM pyruvate. KGDHC, on the other hand, displays incremental increases in NADH and H_2O_2 production with increasing α-ketoglutarate (**Figure 5**). This demonstrates that KGDHC and PDHC, although highly homologous in basic structure, have different kinetic properties in terms of how much substrate is required to induce maximal ROS release. **Figure 5** also demonstrates that H_2O_2 release from KGDHC correlates strongly with NADH production and substrate availability. PDHC on the other does not have the same kinetic characteristics. KGDHC and PDHC also differ in terms of NADH and $O_2^{\bullet-}/H_2O_2$ forming capacity when NAD^+ concentration is varied (**Figure 6**).

By taking advantage of the simultaneous measurement of NADH and H_2O_2, potential site-specific inhibitors for ROS production can be screened. This can help determine the amount of inhibitor that is required to induce maximal inhibition of H_2O_2 release. In addition, by measuring NADH production at the same time, the site for inhibitor action as well as the source of ROS can be identified. Previous studies have shown that the α-ketoglutarate analog, KMV, is highly effective at inhibiting ROS release from KGDHC (≥ 90% inhibition)[13,15]. We also showed that CPI-613, a lipoic acid analog that blocks dihydrolipoamide of the E_2 subunit of PDHC and KGDHC, can also inhibit ROS release from either complex by ~ 90%[13,14]. The site of action for KMV and CPI-613 are shown in **Figure 7**.CPI-613 is a sulfur containing molecule and it is therefore advised that thiol-rich reducing agents (dithiothreitol; DTT) or proteins (albumin) are omitted from the procedure[13]. **Figure 7** demonstrates that both KMV and CPI-613 were both highly effective at limiting both NADH and H_2O_2 by KGDHC. Likewise, CPI-613 completely abolished H_2O_2 release from PDHC (**Figure 7**). Collectively, these results demonstrate that KMV and CPI-613 are highly effective inhibitors for H_2O_2 release and can thus be applied to experiments with isolated mitochondria. Such a screen would be highly beneficial for other potential ROS-forming enzymes since it allows for a direct assessment of the effectiveness and selectivity of different inhibitors on purified flavin-containing dehydrogenases. The simultaneous measurement of NADH also has the added benefit of allowing the preliminary identification of the potential source of ROS within an enzyme complex. **Figure 7** provides a depiction of the catalytic mechanism for KGDHC, which is highly homologous to PDHC. The observation that KMV and CPI-613, which block the E_1 and E_2 subunit of KGDHC, almost completely abolished both H_2O_2 and NADH production, confirms that the E_3 subunit, likely the FAD, is the ROS source[18]. CPI-613 exerted a similar effect on PDHC confirming that the principle site for H_2O_2 release is the E_3 subunit[18]. A similar approach can be used for other dehydrogenases. This would require the identification of inhibitors that block electron flow through different parts of an enzyme complex.

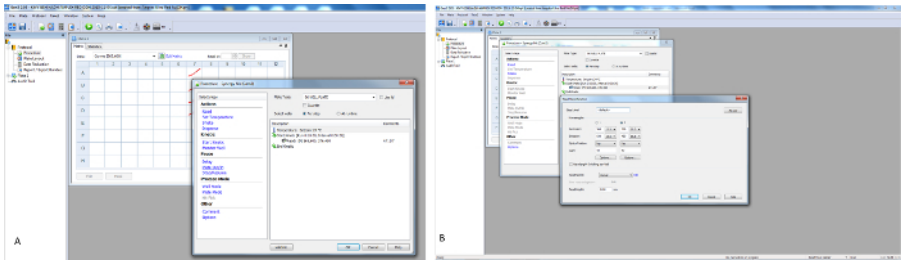

Figure 1: Representative screen shots for assay setup. (**A**) Depiction of procedure set up for the kinetic measurement of changes in NADH and resorufin fluorescence. (**B**) Setting up the fluorescence parameters for the assay. Please click here to view a larger version of this figure.

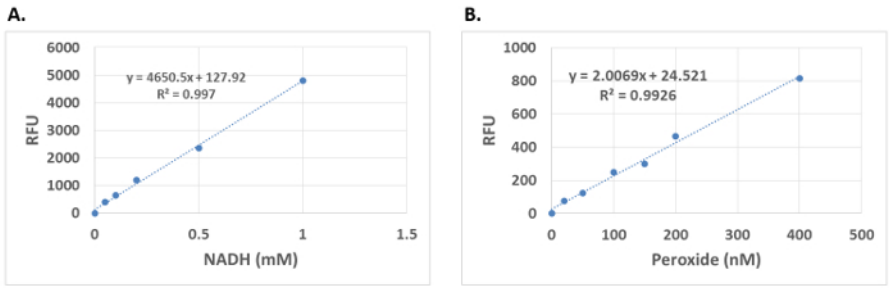

Figure 2: Representative standard curves for NADH and resorufin fluorescence. Curves are utilized to estimate the rate of NADH and $O_2^{\bullet-}/H_2O_2$ production. Please click here to view a larger version of this figure.

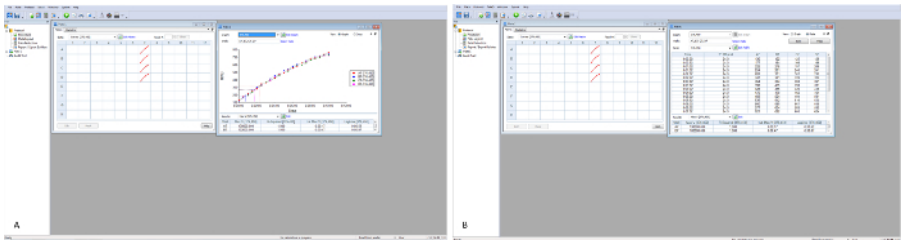

Figure 3: Representative traces for the raw RFU data collected during the assay. (**A**) Curves for each well that was read during the assay. Plate view curves are generated by holding down the CTL button and clicking on each well that is being read. (**B**) For data export, DATA is clicked under VIEW to generate a table containing the representative RFU values. The SPREADSHEET export button is then clicked to export the raw results. Please click here to view a larger version of this figure.

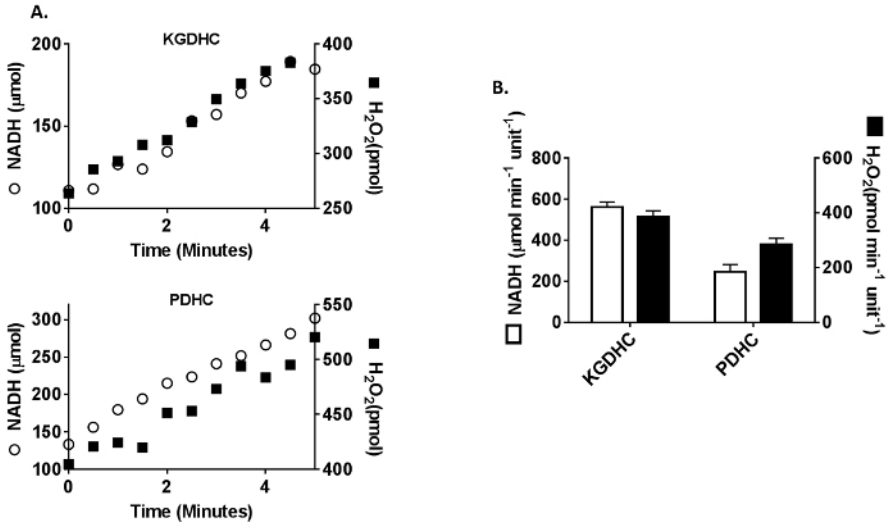

Figure 4: Direct comparison of the H_2O_2 and NADH forming rates of KGDHC and PDHC. (**A**) Simultaneous measurement of H_2O_2 and NADH forming potential of KGDHC and PDHC. (**B**) Calculation of the rate of H_2O_2 and NADH formation by KGDHC and PDHC. Direct comparison of NADH and ROS production by both flavin-containing enzymes demonstrates that KGDHC produces more H_2O_2 which is related to its higher enzymatic capacity. n = 4, mean ± SEM. Please click here to view a larger version of this figure.

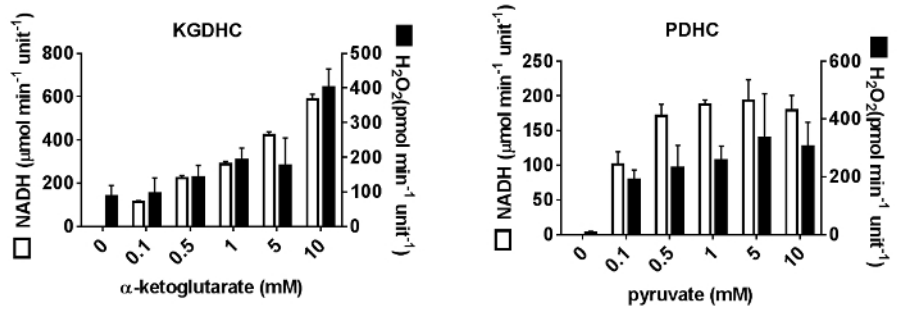

Figure 5: Simultaneous measurement of H_2O_2 and NADH forming rates by KGDHC and PDHC oxidizing different substrate concentrations. Changes in fluorescence were measured as described previously except the final substrate concentration was varied from 0 mM to 10 mM. This approach was used to ascertain the dependency of H_2O_2 release on the kinetic properties of KGDHC and PDHC. n = 4, mean ± SEM. Please click here to view a larger version of this figure.

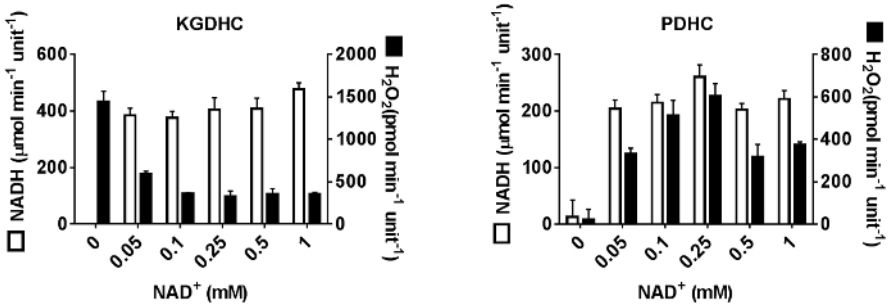

Figure 6: KGDHC and PDHC also display different H_2O_2 and NADH forming properties when NAD^+ levels are changed. Changes in fluorescence were measured as described previously except the final concentration of NAD^+ was varied from 0 mM to 1 mM. This approach was used to ascertain the dependency of H_2O_2 release on the kinetic properties of KGDHC and PDHC. n = 4, mean ± SEM. Please click here to view a larger version of this figure.

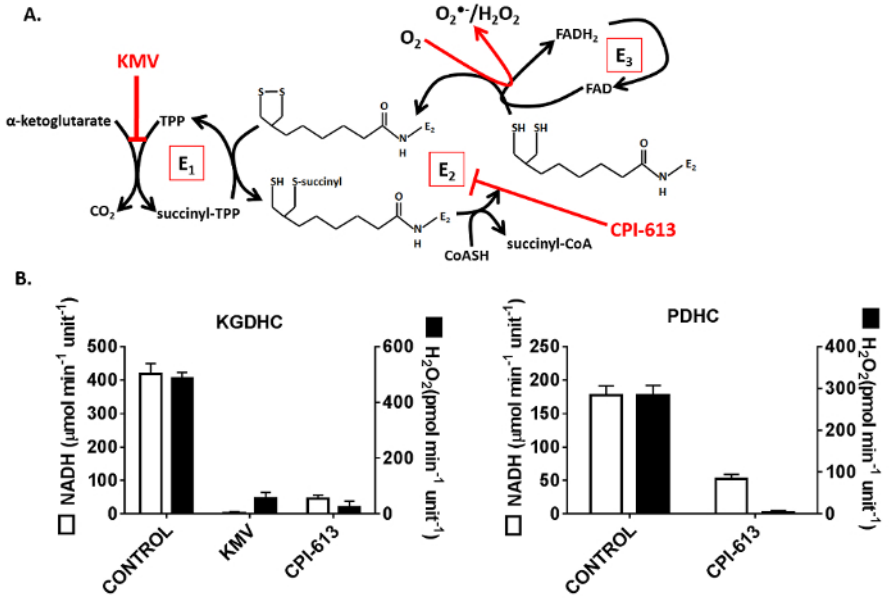

Figure 7: Screening of different site-specific inhibitors for NADH and H_2O_2 production. (**A**) Diagram depicting the catalytic cycle for KGDHC and the sites of action for KMV and CPI-613. Note that PDHC has a homologous catalytic cycle, except that KMV does not compete for the pyruvate binding site. E1: pyruvate or α-ketoglutarate dehydrogenase, E2: dihydrolipoamide acyltransferase, E3: dihydrolipoamide dehydrogenase. (**B**) Effect of KMV and CPI-613 on NADH and H_2O_2 production by KGDHC and PDHC. Samples were preincubated in KMV (10 mM) or CPI-613 (150 µM) and then assayed for NADH and H_2O_2 production. n = 4, mean ± SEM. Please click here to view a larger version of this figure.

Reagent	Working stock concentration	Volume added to well	Final concentration in well
KGDHC or PDHC	1 unit/mL	20 µL	0.1 units/mL
Superoxide dismutase	250 units/mL	20 µL	25 units/mL
Horseradish peroxidase	30 units/mL	20 µL	3 units/mL
Thiamine pyrophosphate	3 mM	20 µL	0.3 mM
Coenzyme A	1 mM	20 µL	0.1 mM
NAD^+	10 mM	20 µL	1 mM
10-Acetyl-3,7-dihydroxyphenoxazine	100 µM	20 µL	10 µM
Substrate	1-100 mM	20 µL	0.1-10 mM

Table 1: Example of a basic protocol set up for the measurement of $O_2^{\bullet-}/H_2O_2$ and NADH production by purified PDH or KGDH. Since 20 µL of each reagent is added to each well and the final volume/reaction is 200 µL, the final concentration of each reagent is 10-fold less than the stock concentration (*e.g.*, the final concentration of NAD^+ in the reaction mixture is 1 mM). Note that reagents should be added to the well in the order presented in the table.

Inhibitor	Target
3-methyl-2-oxo valeric acid	E1 subunit of KGDHC
CPI-613	E2 subunit of oxo acid dehydrogenases

Table 2: List of inhibitors and their targets. Sites of action are also depicted in **Figure 8**.

NADH autofluorescence									
		PDHC				**KGDHC**			
Time	T° 376,450	A1	A2	A3	A4	A5	A6	A7	A8
0:00:04	24.4	99	99	91	88	85	82	58	88
0:00:34	24.4	128	107	99	108	81	80	77	78
0:01:04	24.4	124	128	117	139	97	88	97	76
0:01:34	24.4	146	142	129	132	91	97	84	78
0:02:04	24.4	161	153	148	146	90	107	95	88
0:02:34	24.4	171	160	156	145	97	103	111	122
0:03:04	24.4	176	176	161	169	109	120	99	116
0:03:34	24.4	186	180	179	167	118	123	121	119
0:04:04	24.4	201	182	187	183	127	124	119	131
0:04:34	24.4	225	190	195	186	136	143	124	132
0:05:04	24.4	227	227	203	197	115	143	121	143
Resorufin fluorescence									
		PDHC				**KGDHC**			
Time	T° 565,600	A1	A2	A3	A4	A5	A6	A7	A8
0:00:00	24.4	204	178	169	152	148	113	107	90
0:00:30	24.4	224	188	167	152	144	116	124	112
0:01:00	24.4	212	186	178	161	153	114	122	120
0:01:30	24.4	212	188	165	164	160	132	127	116
0:02:00	24.4	222	203	190	169	154	128	133	127
0:02:30	24.4	217	198	193	179	165	129	147	130
0:03:00	24.4	223	218	202	179	183	142	145	137
0:03:30	24.4	239	223	208	188	179	150	155	148
0:04:00	24.4	236	219	202	183	180	163	156	153
0:04:30	24.4	249	220	214	177	199	149	150	167
0:05:00	24.4	251	232	225	196	211	170	169	161

Table 3: Spreadsheet view of the results collected from the set of experiments. Raw RFU values generated from the experiment are exported to a spreadsheet for further analysis. Using standard curves generated prior to experimentation, the rate of NADH and H_2O_2 production can be calculated in the spreadsheet.

Discussion

This protocol is advantageous since, 1) it eliminates any competing reactions that may otherwise interfere with H_2O_2 detection (*e.g.*, antioxidant systems or other sources of ROS), 2) provides a direct assessment of the native rate of ROS release by a flavin-containing mitochondrial dehydrogenase, 3) allows the comparison of the native ROS release rates of two or more purified flavin-based dehydrogenases, 4) can allow for a direct comparison of the rate of ROS release and enzyme activity, and 5) allows screening of selective competitive inhibitors for ROS release. Our group and others have used this method in previous publications to examine the regulation of ROS by allosteric and redox signaling mechanisms prior to conducting experiments with mitochondria or permeabilized muscle[14,16,17,19,20].

Modifications and Troubleshooting:

This procedure uses basic equipment available at almost every institution. The approach is also low cost and uses common chemicals available through various suppliers. The buffer composition may vary according to enzyme properties - although, we have found that a basic reaction buffer consisting of sucrose, HEPES, mannitol, and EGTA works well in most applications. Raw values for resorufin fluorescence are typically around 50-500 RFU for a ROS releasing enzyme diluted to 0.1 U/mL. Higher RFU values may indicate the AUR reagent has been auto-oxidized

due to exposure to light or repeated freeze-thaw. Therefore, AUR working solutions should be routinely replaced every 2 to 3 weeks (depending on the frequency of use). Impurities in the enzyme preparation or denaturation can lead to lower than normal ROS and NADH readings. Enzyme purity should be routinely monitored by gel electrophoresis. Kinetic properties (Km and Vmax for substrate and NAD^+) should also be assessed immediately after purchase or purification of an enzyme and then routinely monitored thereafter. Most of the reagents used in the assay are stable and can be subjected to multiple freeze-thaw cycles. Pyruvate and α-ketoglutarate should be stored in aliquots of 100 µL at -80 °C to avoid auto-oxidation. Avoid using reducing agents like DTT since it forms $O_2^{\bullet-}/H_2O_2$ directly through radical formation in PDHC and KGDHC (and potentially other flavoenzymes)[17]. Assays can be conducted at 37 °C; however, our group has found that conducting these experiments at 25 °C is ideal for providing more consistent data.

Limitations of the Technique:

One major hurdle associated with this technique is access to purified flavin-containing mitochondrial enzymes. Here, we used commercially available KGDHC and PDHC to demonstrate that this technique can be used to directly compare the ROS release capacity and enzyme activity of flavin-containing mitochondrial dehydrogenases. However, most ROS producing flavin-containing enzymes are not commercially available and must be purified in the laboratory. This can be challenging considering some of these enzymes are membrane bound or absorb to the mitochondrial inner membrane. New protocols for the successful purification of membrane-bound flavin-containing enzymes that produce ROS are now available. This includes purification methods for complex I, complex II, and *sn*-glycerol-3-phosphate dehydrogenase[21,22,23]. Therefore, even though most of the listed ROS generators may not be commercially available, protocols exist for their isolation and purification. The physiological relevance of the results collected using purified flavin-based enzymes is also a limitation. Therefore, findings collected with purified enzymes should be followed up with assays using isolated mitochondria or permeabilized tissue. Five separate studies used this approach to investigate mechanisms for regulation of ROS release by KGDHC and PDHC[14,16,17,19,20]. Preliminary results for the role of redox switches in controlling ROS release were initially tested using purified KGDHC and PDHC, and then mechanisms for regulation were further analyzed in liver and cardiac mitochondria and muscle fiber[14,16,17,20].

Significance with Respect to Existing Methods:

Measuring ROS release from individual sites of production in mitochondria can be challenging due to the presence of competing side reactions that also produce $O_2^{\bullet-}/H_2O_2$ and antioxidant systems that may otherwise lead to the underestimation of native rates. The membrane potential can also alter ROS release rates from various sites and the use of inhibitors can alter electron flow, confounding $O_2^{\bullet-}/H_2O_2$ formation measurements. The method presented here allows the direct evaluation of the ROS release capacity from individual enzymes while simultaneously assessing the relationship between native rates of $O_2^{\bullet-}/H_2O_2$ and enzyme activity. This inexpensive method can serve as a tool for comparing the native ROS release rates for individual flavin-containing mitochondrial enzymes prior to conducting more sophisticated experiments with mitochondria, cells, or tissue. In addition, the method presented herein can be utilized to pre-screen the effectiveness and selectivity of inhibitors for ROS release prior to conducting assays with isolated mitochondria.

Future Applications:

The method presented herein has been used in five separate studies aimed at investigating control over ROS release from PDHC and KGDHC[14,16,17,19,20]. In these studies, inhibitors were screened and ROS release and NADH producing rates were evaluated using purified enzymes. Results collected with the purified enzymes were then verified using isolated mitochondria and permeabilized muscle fibers[14,16,17,20]. Therefore, this method can be applied to a number of future studies aimed at studying native ROS release rates from mitochondria, cells, and muscle fibers.

Critical Steps in the Protocol:

Enzyme purity and its kinetic properties should be routinely monitored. The AUR working stock reagent should also be replaced frequently. This will ensure results collected are consistent. The order of addition of reagents is vital for running a successful experiment (**Table 1**). Inhibitors should be titrated to determine the concentration required to elicit maximum inhibition of ROS release. In this study, we chose 10 mM KMV and 150 µM CPI-613 since we had previously determined that these concentrations induce maximal inhibition of ROS release by KGDHC and PDHC[13].

Disclosures

There is nothing to disclose.

Acknowledgements

This work was funded by the Natural Sciences and Engineering Research Council of Canada (NSERC). Video production was carried out in collaboration with the Center for Innovation in Teaching and Learning (CITL) at Memorial University of Newfoundland.

References

1. Mailloux, R. J. Teaching the fundamentals of electron transfer reactions in mitochondria and the production and detection of reactive oxygen species. *Redox Biol.* **4** 381-398 (2015).
2. Nicholls, D. G. Forty years of Mitchell's proton circuit: From little grey books to little grey cells. *Biochim Biophys Acta.* **1777** (7-8), 550-556 (2008).

3. Brand, M. D. Mitochondrial generation of superoxide and hydrogen peroxide as the source of mitochondrial redox signaling. *Free Radic Biol Med.* **100** 14-31 (2016).
4. Massey, V. Activation of molecular oxygen by flavins and flavoproteins. *J Biol Chem.* **269** (36), 22459-22462 (1994).
5. Mailloux, R. J., Gardiner, D., & O'Brien, M. 2-Oxoglutarate dehydrogenase is a more significant source of O2(.-)/H2O2 than pyruvate dehydrogenase in cardiac and liver tissue. *Free Radic Biol Med.* **97** 501-512 (2016).
6. Sies, H., Berndt, C., & Jones, D. P. Oxidative Stress. *Annu Rev Biochem.* **86** 715-748 (2017).
7. Kuksal, N., Chalker, J., & Mailloux, R. J. Review. Progress in understanding the molecular oxygen paradox - function of mitochondrial reactive oxygen species in cell signaling. *Biol Chem.* (2017).
8. Murphy, M. P. How mitochondria produce reactive oxygen species. *Biochem J.* **417** (1), 1-13 (2009).
9. Wong, H. S., Dighe, P. A., Mezera, V., Monternier, P. A., & Brand, M. D. Production of superoxide and hydrogen peroxide from specific mitochondrial sites under different bioenergetic conditions. *J Biol Chem.* (2017).
10. Harper, M. E., Green, K., & Brand, M. D. The efficiency of cellular energy transduction and its implications for obesity. *Annu Rev Nutr.* **28** 13-33 (2008).
11. Ambrus, A. *et al.* Formation of reactive oxygen species by human and bacterial pyruvate and 2-oxoglutarate dehydrogenase multienzyme complexes reconstituted from recombinant components. *Free Radic Biol Med.* **89** 642-650 (2015).
12. Tretter, L., & Adam-Vizi, V. Generation of reactive oxygen species in the reaction catalyzed by alpha-ketoglutarate dehydrogenase. *J Neurosci.* **24** (36), 7771-7778 (2004).
13. Slade, L. *et al.* Examination of the superoxide/hydrogen peroxide forming and quenching potential of mouse liver mitochondria. *Biochim Biophys Acta.* **1861** (8), 1960-1969 (2017).
14. O'Brien, M., Chalker, J., Slade, L., Gardiner, D., & Mailloux, R. J. Protein S-glutathionylation alters superoxide/hydrogen peroxide emission from pyruvate dehydrogenase complex. *Free Radic Biol Med.* **106** 302-314 (2017).
15. Quinlan, C. L. *et al.* The 2-oxoacid dehydrogenase complexes in mitochondria can produce superoxide/hydrogen peroxide at much higher rates than complex I. *J Biol Chem.* **289** (12), 8312-8325 (2014).
16. Mailloux, R. J., Craig Ayre, D., & Christian, S. L. Induction of mitochondrial reactive oxygen species production by GSH mediated S-glutathionylation of 2-oxoglutarate dehydrogenase. *Redox Biol.* **8** 285-297 (2016).
17. Mailloux, R. J., Gardiner, D., & O'Brien, M. 2-Oxoglutarate dehydrogenase is a more significant source of O2(.-)/H2O2 than pyruvate dehydrogenase in cardiac and liver tissue. *Free Radic Biol Med.* **97** 501-512 (2016).
18. Ambrus, A., & Adam-Vizi, V. Human dihydrolipoamide dehydrogenase (E3) deficiency: Novel insights into the structural basis and molecular pathomechanism. *Neurochem Int.* (2017).
19. Young, A., Gardiner, D., Brosnan, M. E., Brosnan, J. T., & Mailloux, R. J. Physiological levels of formate activate mitochondrial superoxide/hydrogen peroxide release from mouse liver mitochondria. *FEBS Lett.* **591** (16), 2426-2438 (2017).
20. Fisher-Wellman, K. H. *et al.* Mitochondrial glutathione depletion reveals a novel role for the pyruvate dehydrogenase complex as a key H2O2-emitting source under conditions of nutrient overload. *Free Radic Biol Med.* **65** 1201-1208 (2013).
21. Kussmaul, L., & Hirst, J. The mechanism of superoxide production by NADH:ubiquinone oxidoreductase (complex I) from bovine heart mitochondria. *Proc Natl Acad Sci U S A.* **103** (20), 7607-7612 (2006).
22. Huang, L. S., Borders, T. M., Shen, J. T., Wang, C. J., & Berry, E. A. Crystallization of mitochondrial respiratory complex II from chicken heart: a membrane-protein complex diffracting to 2.0 A. *Acta Crystallogr D Biol Crystallogr.* **61** (Pt 4), 380-387 (2005).
23. Yeh, J. I., Chinte, U., & Du, S. Structure of glycerol-3-phosphate dehydrogenase, an essential monotopic membrane enzyme involved in respiration and metabolism. *Proc Natl Acad Sci U S A.* **105** (9), 3280-3285 (2008).

